
Optimal Flow Matching: Learning Straight Trajectories in Just One Step

Nikita Kornilov
MIPT, Skoltech
kornilov.nm@phystech.edu

Petr Mokrov
Skoltech
petr.mokrov@skoltech.ru

Alexander Gasnikov
Innopolis University, Skoltech, MIPT
gasnikov@yandex.ru

Alexander Korotin
Skoltech, AIRI
a.korotin@skoltech.ru

Abstract

Over the several recent years, there has been a boom in development of Flow Matching (FM) methods for generative modeling. One intriguing property pursued by the community is the ability to learn flows with straight trajectories which realize the Optimal Transport (OT) displacements. Straightness is crucial for the fast integration (inference) of the learned flow’s paths. Unfortunately, most existing flow straightening methods are based on non-trivial iterative FM procedures which accumulate the error during training or exploit heuristics based on minibatch OT. To address these issues, we develop and theoretically justify the novel **Optimal Flow Matching** (OFM) approach which allows recovering the straight OT displacement for the quadratic transport in just one FM step. The main idea of our approach is the employment of vector field for FM which are parameterized by convex functions.

1 Introduction

Recent success in generative modeling [Liu et al. \[2023\]](#), [Esser et al. \[2024\]](#), [Cao et al. \[2024\]](#) is mostly driven by Flow Matching (FM) [Lipman et al. \[2022\]](#) models. These models move a known distribution to a target one via ordinary differential equations (ODE) describing the mass movement. However, such processes usually have curved trajectories, resulting in time-consuming ODE integration for sampling. To overcome this issue, researchers developed several improvements of the FM [Liu \[2022\]](#), [Liu et al. \[2022\]](#), [Pooladian et al. \[2023\]](#), which aim to recover more straight paths.

Rectified Flow (RF) method [Liu \[2022\]](#), [Liu et al. \[2022\]](#) iteratively solves FM and gradually rectifies trajectories. Unfortunately, in each FM iteration, it **accumulates the error**, see [\[Liu et al., 2022, §2.2\]](#) and [\[Liu, 2022, §6\]](#). This may spoil the performance of the method. The other popular branch of approaches to straighten trajectories is based on the connection between straight paths and Optimal Transport (OT) [Villani \[2021\]](#). The main goal of OT is to find the way to move one probability distribution to another with the minimal effort. Such OT maps are usually described by ODEs with straight trajectories. In OT Conditional Flow Matching (OT-CFM) [Pooladian et al. \[2023\]](#), [Tong et al. \[2023\]](#), the authors propose to apply FM on top of OT solution between batches from considered distributions. Unfortunately, such a heuristic does not guarantee straight paths because of **minibatch OT biases**, see, e.g., [\[Tong et al., 2023, Figure 1, right\]](#) for the practical illustration.

Contributions. In this paper, we fix the above-mentioned problems of the straightening methods. We propose a novel Optimal Flow Matching (OFM) approach (§3) that after a **single** FM iteration obtains straight trajectories which can be simulated without ODE solving. It recovers OT flow for the quadratic transport cost function, i.e., it solves the Benamou–Brenier problem. We demonstrate the potential of OFM in the series of experiments and benchmarks (§4).

The main idea of our OFM is to consider during FM only specific vector fields which yield straight paths by design. These vector fields are the gradients of convex functions, which in practice are parametrized by Input Convex Neural Networks [Amos et al. \[2017\]](#). In OFM, one can optionally use minibatch OT or any other transport plan as the input, and this is completely theoretically justified.

2 Background and Related Works

In this section, we provide all necessary backgrounds for the theory. First, we recall static (§2.1) and dynamic (§2.2) formulations of Optimal Transport and solvers (§2.3) for them. Then, we recall Flow Matching (§2.4.1) and flow straightening approaches: OT-CFM (§2.4.2) and Rectified Flow (§2.4.3).

Notations. For vectors $x, y \in \mathbb{R}^D$, we denote the inner product by $\langle x, y \rangle$ and the corresponding ℓ_2 norm by $\|x\| := \sqrt{\langle x, x \rangle}$. We use $\mathcal{P}_{2,ac}(\mathbb{R}^D)$ to refer to the set of absolute continuous probability distributions with the finite second moment. For vector $x \in \mathbb{R}^D$ and distribution $p \in \mathcal{P}_{2,ac}(\mathbb{R}^D)$, notation $x \sim p$ means that x is sampled from p . For the push-forward operator, we use symbol $\#$.

2.1 Static Optimal Transport

Monge’s and Kantorovich’s formulations. Consider two distributions $p_0, p_1 \in \mathcal{P}_{2,ac}(\mathbb{R}^D)$ and a cost function $c : \mathbb{R}^D \times \mathbb{R}^D \rightarrow \mathbb{R}$. Monge’s Optimal Transport formulation is given by

$$\inf_{T \# p_0 = p_1} \int_{\mathbb{R}^D} c(x_0, T(x_0)) p_0(x_0) dx_0, \quad (1)$$

where the infimum is taken over measurable functions $T : \mathbb{R}^D \rightarrow \mathbb{R}^D$ which satisfy the mass-preserving constraint $T \# p_0 = p_1$. Such functions are called transport maps. If there exists a transport map T^* that achieves the infimum, then it is called the optimal transport map.

Since the optimal transport map T^* in Monge’s formulation may not exist, there is Kantorovich’s relaxation for problem (1) which addresses this issue. Consider the set of transport plans $\Pi(p_0, p_1)$, i.e., the set of joint distributions on $\mathbb{R}^D \times \mathbb{R}^D$ which marginals are equal to p_0 and p_1 , respectively. Kantorovich’s Optimal Transport formulation is

$$\inf_{\pi \in \Pi(p_0, p_1)} \int_{\mathbb{R}^D \times \mathbb{R}^D} c(x_0, x_1) \pi(x_0, x_1) dx_0 dx_1. \quad (2)$$

With mild assumptions on p_0, p_1 , the infimum is always achieved (possibly not uniquely). An optimal plan $\pi^* \in \Pi(p_0, p_1)$ is called an optimal transport plan. If optimal π^* has the form $[\text{id}, T^*] \# p_0$, then T^* is the solution of Monge’s formulation (1).

Quadratic cost function. In our paper, we mostly consider the quadratic cost function $c(x_0, x_1) = \frac{\|x_0 - x_1\|^2}{2}$. In this case, infimums in both Monge’s and Kantorovich’s OT are always uniquely attained [[Villani, 2021](#), Brenier’s Theorem 2.12]. They are related by $\pi^* = [\text{id}, T^*] \# p_0$. Moreover, the optimal values of (1) and (2) are equal to each other. The square root of the optimal value is called Wasserstein-2 distance $\mathbb{W}_2(p_0, p_1)$ between distributions p_0 and p_1 , i.e.,

$$\mathbb{W}_2^2(p_0, p_1) := \min_{\pi \in \Pi} \int_{\mathbb{R}^D \times \mathbb{R}^D} \frac{\|x_1 - x_0\|^2}{2} \pi(x_0, x_1) dx_0 dx_1 = \min_{T \# p_0 = p_1} \int_{\mathbb{R}^D} \frac{\|x_0 - T(x_0)\|^2}{2} p_0(x_0) dx_0. \quad (3)$$

Dual formulation. For the quadratic cost, problem (3) has the equivalent dual form [Villani \[2021\]](#):

$$\mathbb{W}_2^2(p_0, p_1) = \text{CONST}(p_0, p_1) - \min_{\text{convex } \Psi} \underbrace{\left[\int_{\mathbb{R}^D} \Psi(x_0) p_0(x_0) dx_0 + \int_{\mathbb{R}^D} \bar{\Psi}(x_1) p_1(x_1) dx_1 \right]}_{=: \mathcal{L}_{OT}(\Psi)}, \quad (4)$$

where the minimum is taken over convex functions $\Psi(x) : \mathbb{R}^D \rightarrow \mathbb{R}$. Here $\bar{\Psi}(x_1) := \sup_{x_0 \in \mathbb{R}^D} [\langle x_0, x_1 \rangle - \Psi(x_0)]$ is the convex (Fenchel) conjugate function of Ψ . It is also convex.

The term $\text{CONST}(p_0, p_1)$ does not depend on Ψ . Therefore, the minimization (3) over transport plans π is equivalent to the minimization of $\mathcal{L}_{OT}(\Psi)$ from (4) over convex functions Ψ . Moreover, the optimal transport map T^* can be expressed via an optimal Ψ^* called *Brenier potential* [Villani \[2021\]](#), namely,

$$T^* = \nabla \Psi^*. \quad (5)$$

2.2 Dynamic Optimal Transport

In [Benamou and Brenier \[2000\]](#), the authors show that the calculation of Optimal Transport map in (3) for the quadratic cost can be equivalently reformulated in a dynamic form. This form operates with a vector fields defining time-dependent mass transport instead of just static transport maps.

Preliminaries. We consider the fixed time interval $[0, 1]$. Let $u(t, \cdot) \equiv u_t(\cdot) : [0, 1] \times \mathbb{R}^D \rightarrow \mathbb{R}^D$ be a vector field and $\{\{z_t\}_{t \in [0, 1]}\}$ be the set of random trajectories such that for each trajectory $\{z_t\}_{t \in [0, 1]}$ the starting point z_0 is sampled from p_0 and z_t satisfies the differential equation

$$dz_t = u_t(z_t)dt, \quad z_0 \sim p_0. \quad (6)$$

In other words, the trajectory $\{z_t\}_{t \in [0, 1]}$ is defined by its initial point $z_0 \sim p_0$ and goes along the speed vector $u_t(z_t)$. Under mild assumptions on u , for each initial z_0 , the trajectory is unique.

Let $\phi^u(t, \cdot) \equiv \phi_t^u(\cdot) : [0, 1] \times \mathbb{R}^D \rightarrow \mathbb{R}^D$ denote the flow map, i.e., it is the function that maps the initial z_0 to its position at moment of time t according to the ODE (6), i.e.,

$$d\phi_t^u(z_0) = u_t(\phi_t^u(z_0)), \quad \phi_0^u(z_0) = z_0. \quad (7)$$

If initial points z_0 of trajectories are distributed according to p_0 , then (6) defines a distribution p_t of z_t at time t , which can be expressed via with the push-forward operator, i.e., $p_t := \phi_t^u \# p_0$.

Benamou–Brenier problem. Dynamic OT is the following minimization problem:

$$\begin{aligned} \mathbb{W}_2^2(p_0, p_1) = \inf_u & \int_0^1 \int_{\mathbb{R}^D} \frac{\|u_t(x)\|_2^2}{2} \underbrace{\phi_t^u \# p_0(x)}_{:= p_t(x)} dx dt, \\ \text{s.t.} & \quad \phi_1^u \# p_0 = p_1. \end{aligned} \quad (8)$$

In (8), we look for the vector fields u that define the flows which start at p_0 and end at p_1 . Among such flows, we seek for one which has the minimal kinetic energy over the entire time interval.

There is a connection between the static OT map $T^* = \nabla \Psi^*$ and the dynamic OT solution u^* . Namely, for every initial point z_0 , the vector field u^* defines a linear trajectory $\{z_t\}_{t \in [0, 1]}$:

$$z_t = t \nabla \Psi^*(z_0) + (1 - t)z_0, \quad \forall t \in [0, 1]. \quad (9)$$

2.3 Continuous Optimal Transport Solvers

There exist a variety of continuous OT solvers [Genevay et al. \[2016\]](#), [Seguy et al. \[2017\]](#), [Taghvaei and Jalali \[2019\]](#), [Makkuva et al. \[2020\]](#), [Fan et al. \[2020\]](#), [Daniels et al. \[2021\]](#), [Vargas et al. \[2021\]](#), [De Bortoli et al. \[2021\]](#), [Korotin et al. \[2021b\]](#), [Rout et al. \[2022\]](#), [Liu et al. \[2022\]](#), [Korotin et al. \[2023c,b\]](#), [Choi et al. \[2023\]](#), [Fan et al. \[2023\]](#), [Uscidda and Cuturi \[2023\]](#), [Amos \[2023\]](#), [Tong et al. \[2023\]](#), [Gushchin et al. \[2024b\]](#), [Mokrov et al. \[2024\]](#), [Asadulaev et al. \[2024\]](#). For a survey of solvers designed for OT with quadratic cost, see [Korotin et al. \[2021a\]](#). In this paper, we focus only on the most relevant ones, called the ICNN-based solvers [Taghvaei and Jalali \[2019\]](#), [Korotin et al. \[2019\]](#), [Makkuva et al. \[2020\]](#), [Amos \[2023\]](#). These solvers directly minimize objective \mathcal{L}_{OT} from (4) parametrizing a class of convex functions with convex in input neural networks called ICNNs [Amos et al. \[2017\]](#) (for more details, see ‘‘Parametrization of Ψ ’’ in §3.2). Solvers details may differ, but the main idea remains the same. To calculate the conjugate function $\bar{\Psi}(x_1)$ at the point x_1 , they solve the convex optimization problem from conjugate definition. Envelope Theorem [Afriat \[1971\]](#) allows obtaining closed-form formula for the gradient of the loss.

2.4 Flow Matching Framework

In this section, we recall popular approaches [Liu et al. \[2022\]](#), [Liu \[2022\]](#), [Pooladian et al. \[2023\]](#) to find fields u which transport a given probability distribution p_0 to a target p_1 and their relation to OT.

2.4.1 Flow Matching (FM)

To find such a field, one samples points x_0, x_1 from a transport plan $\pi \in \Pi(p_0, p_1)$, e.g., the independent plan $p_0 \times p_1$. The vector field u is encouraged to follow the direction $x_1 - x_0$ of the linear interpolation $x_t = (1 - t)x_0 + tx_1$ at any moment $t \in [0, 1]$, i.e., one solves:

$$\min_u \mathcal{L}_{FM}^\pi(u) := \int_0^1 \left\{ \int_{\mathbb{R}^D \times \mathbb{R}^D} \|u_t(x_t) - (x_1 - x_0)\|^2 \pi(x_0, x_1) dx_0 dx_1 \right\} dt, \quad x_t = (1 - t)x_0 + tx_1. \quad (10)$$

We denote the solution of (10) and the corresponding flow map (7) by u^π and ϕ^π , respectively.

The intuition of this procedure is as follows: linear interpolation $x_t = (1-t)x_0 + tx_1$ is an intuitive way to move p_0 to p_1 , but it requires knowing x_1 . By fitting u with the direction $x_1 - x_0$, one yields the vector field that can construct this interpolation without any information about x_1 .

The set of trajectories $\{\{z_t\}_{t \in [0,1]}\}$ generated by u_t^π (with $z_0 \sim p_0$) has a useful property: the flow map ϕ_1^π transforms distribution p_0 to distribution p_1 for any initial transport plan π . Moreover, marginal distribution $p_t = \phi_t^\pi \# p_0$ is equal to the distribution of linear interpolation $x_t = (1-t)x_0 + tx_1$ for any t and $x_0, x_1 \sim \pi$. This feature is called marginal preserving property.

To push point x_0 according to learned u , one needs to integrate ODE (6) via numerical solvers. The vector fields with straight (or nearly straight) paths incur much smaller time-discretization error and increase effectiveness of computations, which is in high demand for applications.

Researchers noticed that some initial plans π can result in more straight paths after FM rather than the standard independent plan $p_0 \times p_1$. The two most popular approaches to choose better plans are Optimal Transport Conditional Flow Matching Pooladian et al. [2023], Tong et al. [2023] and Rectified Flow Liu et al. [2022].

2.4.2 Optimal Transport Conditional Flow Matching (OT-CFM)

If one uses the OT plan π^* as the initial plan for FM, then it returns the Brenier’s vector field u^* which generates exactly straight trajectories (9). However, typically, the true OT plan π^* is not available. In such a case, in order to achieve some level of straightness in the learned trajectories, a natural idea is to take the initial plan π to be close to the optimal π^* . Inspired by this, the authors of OT-CFM Pooladian et al. [2023], Tong et al. [2023] take the advantage of minibatch OT plan approximation. Firstly, they independently sample batches of points from p_0 and p_1 . Secondly, they join the batches together according to the discrete OT plan between them. The resulting joined batch is then used in FM.

The main drawback of OT-CFM is that it recovers only biased dynamic OT solution. In order to converge to the true transport plan the batch size should be large [Bernton et al., 2019], while with a growth of batch size computational time increases drastically [Tupitsa et al., 2022]. In practice, batch sizes that ensure approximation good enough for applications are nearly infeasible to work with.

2.4.3 Rectified Flow (RF)

In Liu et al. [2022], the authors propose an iterative approach to refine the plan π , straightening the trajectories more and more with each iteration. Formally, Flow Matching procedure denoted by FM takes the transport plan π as input and returns an optimal flow map via solving (10):

$$\phi^\pi := \text{FM}(\pi). \quad (11)$$

One can iteratively apply FM to the initial transport plan (e.g., the independent plan), gradually rectifying it. Namely, Rectified Flow Algorithm on K -th iteration has update rule

$$\phi^{K+1} = \text{FM}(\pi^K), \quad \pi^{K+1} = [\text{id}, \phi^{K+1}] \# p_0, \quad (12)$$

where ϕ^K, π^K denote flow map and transport plan on K -th iteration, respectively.

The trajectories $\{\{z_t\}_{t \in [0,1]}\}^K$ generated after K iteration of Rectified Flow provably become more and more straight, i.e., error in approximation $z_t^K \approx (1-t)z_0^K + tz_1^K, \forall t \in [0, 1]$ decreases with K .

The authors also notice that for any convex cost function c the flow map ϕ_1^π from Flow Matching yields lower or equal transport cost than initial transport plan π :

$$\int_{\mathbb{R}^D} c(x_0, \phi_1^\pi(x_0)) p_0(x_0) dx_0 \leq \int_{\mathbb{R}^D \times \mathbb{R}^D} c(x_0, x_1) \pi(x_0, x_1) dx_0 dx_1. \quad (13)$$

Intuitively, the transport costs are guaranteed to decrease because the trajectories of FM as solutions of well-defined ODE do not intersect each other, even if the initial lines connecting x_0 and x_1 can.

With each iteration of RF (12), transport costs for all convex cost functions do not increase, but, for a given cost function, convergence to its own OT plan is not guaranteed. In Liu [2022], the authors address this issue and, for any particular convex cost function c , modify Rectified Flow to converge to OT map for c . In this modification, called c -Rectified Flow (c -RF), the authors slightly change the FM training objective and restrict the optimization domain only to potential vector fields

$u_t(\cdot) = \nabla \bar{c}(\nabla f_t(\cdot))$, where $f_t(\cdot) : \mathbb{R}^D \rightarrow \mathbb{R}$ is an arbitrary time-dependent scalar valued function and \bar{c} is the convex conjugate of the cost function c . In case of the quadratic cost function, the training objective remains the same, and the vector field u_t is set as the simple gradient $\nabla f_t(\cdot)$ of the scalar valued function f_t .

Unfortunately, in practice, with each iteration (c -)RF accumulates error caused by inexactness from previous iterations, the issue mentioned in [Liu, 2022, §6, point 3]. Due to neural approximations, we can not get exact solution of FM (e.g., $\phi_1^K \# p_0 \neq p_1$), and this inexactness only grows with iterations. In addition, training of (c -)RF becomes non-simulation free after the first iteration, since to calculate the plan $\pi^{K+1} = [\text{id}, \phi^{K+1}] \# p_0$ it has to integrate ODE.

3 Optimal Flow Matching (OFM)

In this section, we provide the design of our novel Optimal Flow Matching algorithm (1) that fixes main problems of Rectified Flow and OT-CFM approaches described above. In theory, it obtains exactly **straight trajectories** and recovers the unbiased optimal transport map for the quadratic cost **just in one FM iteration** with **any** initial transport plan. Moreover, during inference, OFM does not require solving ODE to transport points.

We discuss theory behind our approach (§3.1), its practical implementation aspects (§3.2) and the relation to prior works (§3.3). All proofs are located in Appendix A.

3.1 Theory: Deriving the Optimization Loss

Consider the quadratic cost function $c(x_0, x_1) = \frac{\|x_0 - x_1\|^2}{2}$. We aim to solve the Benamou–Brenier problem (8) between distributions p_0 and p_1 and construct the dynamic OT field u^* , since it generates straight trajectories. The main idea of our Optimal Flow Matching (OFM) is to minimize the Flow Matching loss (10) not over all possible vector fields u , but only over specific *optimal* ones, which yield straight paths by construction and include desired dynamic OT field u^* .

Optimal vector fields. We say that a vector field u^Ψ is optimal if it generates linear trajectories $\{\{z_t\}_{t \in [0,1]}\}$ such that there exist a convex function $\Psi : \mathbb{R}^D \rightarrow \mathbb{R}$, which for any path $\{z_t\}_{t \in [0,1]}$ pushes the initial point z_0 to the final one as $z_1 = \nabla \Psi(z_0)$, i.e.,

$$z_t = (1-t)z_0 + t\nabla \Psi(z_0), \quad t \in [0, 1].$$

The function Ψ defines the ODE

$$dz_t = (\nabla \Psi(z_0) - z_0)dt, \quad z_t|_{t=0} = z_0. \quad (14)$$

Equation (14) does not provide a closed formula for u^Ψ as it depends on z_0 . The explicit formula is constructed as follows: for a time $t \in [0, 1]$ and point x_t , we can find a trajectory $\{z_t\}_{t \in [0,1]}$ s.t.

$$x_t = z_t = (1-t)z_0 + t\nabla \Psi(z_0) \quad (15)$$

and recover the initial point z_0 . We postpone the solution of this problem to §3.2. For now, we define the inverse of flow map (7) as $(\phi_t^\Psi)^{-1}(x_t) := z_0$ and the vector field $u_t^\Psi(x_t) := \nabla \Psi(z_0) - z_0 = \nabla \Psi((\phi_t^\Psi)^{-1}(x_t)) - (\phi_t^\Psi)^{-1}(x_t)$, which generates ODE (14), i.e., $dz_t = u_t^\Psi(z_t)dt$. The concept of optimal vector fields is depicted on Figure 1.

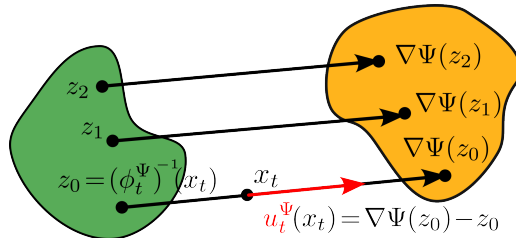


Figure 1: Optimal Vector Fields.

We highlight that the solution of dynamic OT lies in the class of optimal vector fields, since it generates linear trajectories (9) with the Brenier potential Ψ^* (5).

Training objective. Our Optimal Flow Matching (OFM) approach is as follows: we restrict the optimization domain of FM (10) with fixed plan π only to the optimal vector fields. We put the formula for the vector field u_Ψ into FM loss from (10) and define our Optimal Flow Matching loss:

$$\mathcal{L}_{OFM}^\pi(\Psi) := \mathcal{L}_{FM}^\pi(u^\Psi) = \int_0^1 \left\{ \int_{\mathbb{R}^D \times \mathbb{R}^D} \|u_t^\Psi(x_t) - (x_1 - x_0)\|^2 \pi(x_0, x_1) dx_0 dx_1 \right\} dt, \quad (16)$$

$$x_t = (1-t)x_0 + tx_1.$$

Proposition 1 (Simplified OFM Loss). *We can simplify (16) to a more suitable form:*

$$\mathcal{L}_{OFM}^\pi(\Psi) = \int_0^1 \left\{ \int_{\mathbb{R}^D \times \mathbb{R}^D} \left\| \frac{(\phi_t^\Psi)^{-1}(x_t) - x_0}{t} \right\|^2 \pi(x_0, x_1) dx_0 dx_1 \right\} dt, \quad x_t = (1-t)x_0 + tx_1. \quad (17)$$

The simplified form (17) gives a hint for understanding of OFM loss: it measures how well Ψ restores initial points x_0 of linear interpolations depending on future point x_t and time t . The main technical result, which is used to derive the main properties of OFM, is presented in Lemma 1.

Lemma 1 (Main Integration Lemma). *For any two points $x_0, x_1 \in \mathbb{R}^D$ and a convex function Ψ , the following equality holds true:*

$$\int_0^1 \|u_t^\Psi(x_t) - (x_1 - x_0)\|^2 dt = 2 \cdot [\Psi(x_0) + \bar{\Psi}(x_1) - \langle x_0, x_1 \rangle]. \quad (18)$$

The proof that integration over time in case of linear interpolation can be calculated analytically for any x_0, x_1, Ψ via fancy formula (18) is not trivial and requires tricky integration techniques. As a consequence of Lemma 1, minimization of OFM loss (16) over Ψ recovers desired dynamic OT.

Theorem 1 (OFM and OT connection). *Let us consider two distributions $p_0, p_1 \in \mathcal{P}_{ac,2}(\mathbb{R}^D)$ and any transport plan $\pi \in \Pi(p_0, p_1)$ between them. Then, losses $\mathcal{L}_{OT}(\Psi)$ and $\mathcal{L}_{OFM}^\pi(\Psi)$, defined in (4) and (16), respectively, have the same minimizers, i.e.,*

$$\arg \min_{\text{convex } \Psi} \mathcal{L}_{OFM}^\pi(\Psi) = \arg \min_{\text{convex } \Psi} \mathcal{L}_{OT}(\Psi).$$

Generative properties of OFM. In this paragraph, we provide another view on our OFM approach. In our OFM, we wish to construct a vector field u close to the dynamic OT field u^* . We can use the least square regression to measure the distance between them:

$$\text{DIST}(u, u^*) := \int_0^1 \int_{\mathbb{R}^D} \|u_t(x_t) - u_t^*(x_t)\|^2 \underbrace{\phi_t^* \# p_0(x_t)}_{:= p_t^*(x_t)} dx_t dt. \quad (19)$$

Proposition 2 (Intractable Distance). *The distance $\text{DIST}(u, u^*)$ between an arbitrary vector field u and OT field u^* equals to the FM loss from (10) with the optimal plan π^* , i.e.,*

$$\text{DIST}(u, u^*) = \mathcal{L}_{FM}^{\pi^*}(u) - \underbrace{\mathcal{L}_{FM}^{\pi^*}(u^*)}_{=0}.$$

We can not minimize intractable $\text{DIST}(u, u^*)$ since the optimal plan π^* is unknown. In OT-CFM Tong et al. [2023], authors heuristically approximate π^* in $\mathcal{L}_{FM}^{\pi^*}(u)$, but obtain biased solution. Surprisingly, for the *optimal* vector fields, the distance can be calculated explicitly via **any** known plan π .

Proposition 3 (Tractable Distance For OFM). *The distance $\text{DIST}(u^\Psi, u^{\Psi^*})$ between an **optimal** vector field u^Ψ generated by a convex function Ψ and the vector field u^{Ψ^*} with the Brenier potential Ψ^* can be evaluated directly via OFM loss (16) and **any** plan π :*

$$\text{DIST}(u^\Psi, u^{\Psi^*}) = \mathcal{L}_{FM}^\pi(u^\Psi) - \mathcal{L}_{FM}^\pi(u^{\Psi^*}) = \mathcal{L}_{OFM}^\pi(\Psi) - \mathcal{L}_{OFM}^\pi(\Psi^*).$$

In (31), the first term is our tractable OFM loss, and the second term does not depend on Ψ . Hence, during the whole minimization process in our OFM, we gradually lower the distance (19) between the current vector field and the dynamic OT field up to the complete match.

3.2 Practical implementation aspects

In this subsection, we explain the details of optimization of our Optimal Flow Matching loss (16).

Flow map inversion. In order to find the initial point $z_0 = (\phi_t^\Psi)^{-1}(x_t)$, we note that (15)

$$x_t = (1-t)z_0 + t\nabla\Psi(z_0)$$

is equivalent to

$$\nabla \left(\frac{(1-t)}{2} \|\cdot\|^2 + t\Psi(\cdot) - \langle x_t, \cdot \rangle \right) (z_0) = 0.$$

The function under gradient operator ∇ has minimum at the required point z_0 , since at z_0 the gradient of it equals 0. If $t < 1$ the function is at least $(1-t)$ -strongly convex, and the minimum is unique. The case $t = 1$ is negligible in practice, since it has zero probability to appear during training.

We can reduce the problem of inversion to the following minimization subproblem

$$(\phi_t^\Psi)^{-1}(x_t) = \arg \min_{z_0 \in \mathbb{R}^D} \left[\frac{(1-t)}{2} \|z_0\|^2 + t\Psi(z_0) - \langle x_t, z_0 \rangle \right]. \quad (20)$$

Optimization subproblem (20) is at least $(1-t)$ -**strongly convex** and can be effectively solved for any given point x_t (in comparison with typical non-convex optimization).

Parametrization of Ψ . In practical implementation, we parametrize the class of convex functions with Input Convex Neural Networks (ICNNs) Amos et al. [2017] Ψ_θ and parameters θ . These are scalar-valued neural networks built in such a way that the network is convex in inputs. They consist of fully-connected or convolution blocks, some weights of which are set to be non-negative in order to keep convexity. In addition, activation functions are considered to be only non-decreasing and convex in each input coordinate. These networks are able to support most of the popular training techniques (e.g., gradient descent optimization, dropout, skip connection etc.). In Appendix C, we discuss used architectures.

OFM loss calculation. The calculation of OFM loss (16) requires solving the minimization subproblem (20). Due to it, here we provide an explicit formula for gradient of (16), such that it does not contain the gradient of $(\phi_t^{\Psi_\theta})^{-1}$ w.r.t. parameters θ .

Proposition 4 (Explicit Loss Gradient Formula). *The gradient of \mathcal{L}_{OFM}^π can be calculated as*

$$z_0 = \text{NO-GRAD} \left\{ (\phi_t^{\Psi_\theta})^{-1}(x_t) \right\},$$

$$\frac{d\mathcal{L}_{OFM}^\pi}{d\theta} := \frac{d}{d\theta} \mathbb{E}_{t; x_0, x_1 \sim \pi} \left\langle \text{NO-GRAD} \left\{ 2 \left(t \nabla^2 \Psi_\theta(z_0) + (1-t)I \right)^{-1} \frac{(x_0 - z_0)}{t} \right\}, \nabla \Psi_\theta(z_0) \right\rangle,$$

where variables under NO-GRAD remain constants during differentiation.

Algorithm. The Optimal Flow Matching pseudocode is presented in 1. We estimate math expectation over plan π and time t with uniform distribution on $[0, 1]$ via unbiased Monte Carlo estimate.

Algorithm 1 Optimal Flow Matching

Input: Initial transport plan $\pi \in \Pi(p_0, p_1)$, number of iterations K , batch size B , optimizer Opt , sub-problem optimizer $subOpt$, ICNN Ψ_θ

- 1: **for** $k = 0, \dots, K - 1$ **do**
- 2: Sample batch $\{(x_0^i, x_1^i)\}_{i=1}^B$ of size B from plan π ;
- 3: Sample times batch $\{t^i\}_{i=1}^B$ of size B from $U[0, 1]$;
- 4: Calculate linear interpolation $x_{t^i}^i = (1 - t^i)x_0^i + t^i x_1^i$ for all $i \in \overline{1, B}$;
- 5: Find the initial points z_0^i via solving the convex problem with $subOpt$:

$$z_0^i = \text{NO-GRAD} \left\{ \arg \min_{z_0^i} \left[\frac{(1-t^i)}{2} \|z_0^i\|^2 + t^i \Psi_\theta(z_0^i) - \langle x_{t^i}^i, z_0^i \rangle \right] \right\};$$

- 6: Calculate loss $\hat{\mathcal{L}}_{OFM}$

$$\hat{\mathcal{L}}_{OFM} = \frac{1}{B} \sum_{i=1}^B \left\langle \text{NO-GRAD} \left\{ 2 \left(t^i \nabla^2 \Psi_\theta(z_0^i) + (1-t^i)I \right)^{-1} \frac{(x_0^i - z_0^i)}{t^i} \right\}, \nabla \Psi_\theta(z_0^i) \right\rangle;$$

- 7: Update parameters θ via optimizer Opt step with $\frac{d\hat{\mathcal{L}}_{OFM}}{d\theta}$;
 - 8: **end for**
-

3.3 Relation to Prior Works

In this subsection, we compare our Optimal Flow Matching and previous straightening approaches. One unique feature of OFM is that it works only with flows which have straight paths by design and does not require ODE integration to transport points. Other methods may result in non-straight paths during training, and they still have to solve ODE even with near-straight paths.

OT-CFM Pooladian et al. [2023], Tong et al. [2023]. Unlike our OFM approach, OT-CFM method retrieves biased OT solution, and the recovery of straight paths is not guaranteed. In OT-CFM, minibatch OT plan appears as a heuristic that helps to get better trajectories in practice. In contrast, usage of **any** initial transport plan π in our OFM is completely justified in Theorem 1.

Rectified Flow Liu et al. [2022], Liu [2022]. In Rectified Flows Liu et al. [2022], the authors iteratively apply Flow Matching to refine the obtained trajectories. However, in each iteration, RF accumulates error since one may not learn the exact flow due to neural approximations. In addition, RF does not guarantee convergence to the OT plan for the quadratic cost. The c -Rectified Flow Liu [2022] modification can converge to the OT plan for any cost function c , but still remains iterative. In addition, RF and c -RF both requires ODE simulation after the first iteration to continue training. In OFM, we work only with the quadratic cost function, but retrieve its OT solution in **just one FM iteration** without simulation of the trajectories.

Light and Optimal Schrödinger Bridge. In Gushchin et al. [2024a], the authors observe the relation between Entropic Optimal Transport (EOT) Léonard [2013], Chen et al. [2016] and Bridge Matching (BM) Shi et al. [2024] problems. These are stochastic analogs of OT and FM, respectively. In EOT and BM, instead of deterministic ODE and flows, one considers stochastic processes with non-zero stochasticity. The authors prove that, during BM, one can restrict considered processes only to the specific ones and retrieve the solution of EOT. Hypothetically, our OT/FM case is a limit of their EOT/BM case when the stochasticity tends to zero. Proofs in Gushchin et al. [2024a] for EOT are based on sophisticated KL divergence properties. We do not know whether our results for OFM can be derived by taking the limit of their stochastic case. To derive the properties of our OFM, we use **completely different proof techniques** based on computing integrals over curves rather than KL-based techniques. Besides, in practice, the authors of Gushchin et al. [2024a] mostly focus on Gaussian mixture parametrization while our method allows using neural networks (ICNNs).

4 Experimental Illustrations

In this section, we showcase the performance of our proposed OFM method on illustrative 2D scenario (§4.1) and Wasserstein-2 benchmark Korotin et al. [2021a] (§4.2). Finally, we apply our approach for solving high-dimensional unpaired image-to-image translation in the latent space of pretrained ALAE autoencoder (§4.3). Our PyTorch code will be made public once the paper will be accepted. The technical details of our experiments (architectures, hyperparameters) are in the Appendix C.

4.1 Illustrative 2D Example

We illustrate the proof-of-concept of our Optimal Flow Matching on 2D setup. We solve the OT between a standard Gaussian $p_0 = \mathcal{N}(0, I)$ and a Mixture of eight Gaussians p_1 depicted in the Figure 2a. We run our Algorithm 1 for different stochastic plans π : independent plan $p_0 \times p_1$ (Figure 2b), minibatch and *antiminibatch* (Figures 2c, 2d) discrete OT (quadratic cost) with batch size $B_{\text{mb}} = 64$. In the *antiminibatch* case, we compose the pairs of source and target points by solving discrete OT with **minus** quadratic cost $-\|x - y\|_2^2$. The fitted OFM maps and trajectories are presented in Figure 2. We empirically see that our OFM finds the *same solution for all considered initial plans* π .

4.2 High-dimensional OT Benchmarks

To compare our OFM with other FM based methods and OT solvers, we run OT Benchmark Korotin et al. [2021a]. The authors provide high-dimensional continuous distributions p_0, p_1 for which the ground truth OT map T^* for the quadratic cost is known by the construction. To assess the quality of retrieved transport maps, we use standard *unexplained variance percentage* \mathcal{L}^2 -UVP Korotin et al. [2019] metric.

Solvers. We evaluate Flow Matching (FM), Conditional Flow Matching (OT-CFM), Rectified Flow (RF), c -Rectified Flow (c -RF) and the most relevant OT solver MMv-1 Stanczuk et al. [2021]. In

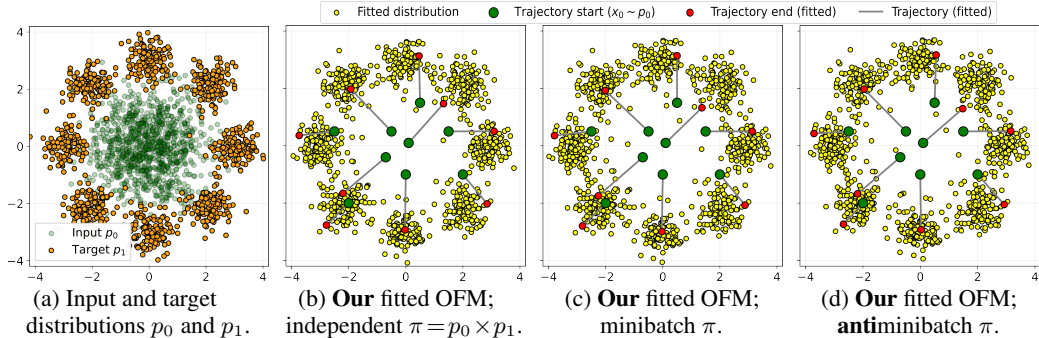


Figure 2: Performance of **our** Optimal Flow Matching on *Gaussian*→*Eight Gaussians* 2D setup.

MMv-1, the authors directly minimize the dual formulation loss \mathcal{L}_{OT} (4) by parametrizing Ψ with ICNNs and calculating $\bar{\Psi}(x_1)$ via convex optimization subproblem. The latter is similar to our inversion (20). We also provide results for linear map which translates means and variances of distributions to each other.

We consider 2 initial plans: independent plan (Ind) and minibatch OT (MB), the batch size for the latter is $B_{mb} = 64$. The results are presented in Table 1. More details are given in Appendix C.1.

Solver	Solver type	$D=2$	$D=4$	$D=8$	$D=16$	$D=32$	$D=64$	$D=128$	$D=256$
MMv1* Stanczuk et al. [2021]	Dual OT solver	0.2	1.0	1.8	1.4	6.9	8.1	2.2	2.6
Linear* Korotin et al. [2019]	Baseline	14.1	14.9	27.3	41.6	55.3	63.9	63.6	67.4
OT-CFM Tong et al. [2023]		0.16	0.73	2.27	4.33	7.9	11.4	12.1	27.5
RF Liu et al. [2022]		8.58	49.46	51.25	63.33	63.52	85.13	84.49	83.13
c-RF Liu [2022]		1.56	13.11	17.87	35.39	48.46	66.52	68.08	76.48
OFM Ind (Ours)	Flow Matching	0.4	1.1	2.01	2.56	4.5	11.31	9.83	16.12
OFM MB (Ours)		0.33	0.81	1.53	1.96	3.35	10.13	6.68	11.65

Table 1: \mathcal{L}^2 -UVP values of solvers fitted on high-dimensional benchmarks in dimensions $D = 2, 4, 8, 16, 32, 64, 128, 256$. The best metric over *Flow Matching* solvers is **bolded**. *Metrics for MMv1 and linear baseline are taken from Korotin et al. [2019].

Results. Among FM-based methods, OFM with any plan demonstrates the best results when $D > 4$. For all plans, OFM convergences to close final solutions and metrics. Minibatch plan provides a bit better results, especially in high dimensions. In theory, the OFM results for any plan π must be similar. However, in stochastic optimization, plans with large variance yield convergence to slightly worse solutions.

MMv1 beats OFM in some dimensions. MMv1 is designed to solve OT via simple map, while OFM deals with vector fields and have to consider whole time interval $[0, 1]$. RF demonstrates worse performance than even linear baseline, but is ok since it is not designed to solve \mathbb{W}_2 OT. In turn, c-RF works better, but rapidly deteriorates with increasing dimensions. OT-CFM demonstrates the best results among baseline FM-based methods, but still underperforms compared to our OFM solver in high dimensions.

4.3 Unpaired Image-to-image Transfer

Another task that involves learning a translation between two distributions is unpaired image-to-image translation [Zhu et al., 2017]. We follow the setup of Korotin et al. [2023a] where translation is computed in the 512 dimensional latent space of the pre-trained ALAE autoencoder Pidhorskyi et al. [2020] on 1024×1024 FFHQ dataset [Karras et al., 2019]. In particular, we split the train FFHQ sample (60K faces) into *children* and *adults* subsets and consider the corresponding ALAE latent codes as the source and target distributions p_0 and p_1 . At the inference stage, we take a new (unseen) *adult* face from a test FFHQ sample, extract its latent code, process with our learned model and then

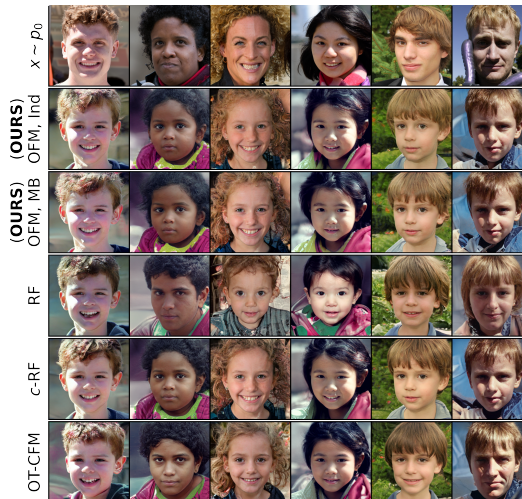


Figure 3: Unpaired I2I *Adult*→*Child* by FM solvers, ALAE 1024×1024 FFHQ latent space.

decode back to the image space. Our obtained qualitative results are presented in Figure 3. The batch size for minibatch OT methods ([OFM, MB], [OT-CFM]) is $B_{\text{mb}} = 128$. Our OFM converges to nearly the same solution for both independent and MB plans and demonstrates qualitatively plausible translations. The most similar results to our method are demonstrated by [c-RF]. Similar to OFM, this method (in the limit of RF steps) also recovers the quadratic OT mapping.

5 Discussion

Potential impact. We believe that our novel theoretical results have a huge potential for improving modern straightening methods and inspiring the community for further studies. The direct connection with well-studied Optimal Transport may result in adopting of OT’s strong sides to Flow Matching and deepening the understanding of it. We think this is of high importance especially taking into account that modern generative models start to extensively use flow matching methods [Yan et al. \[2024\]](#), [Liu et al. \[2023\]](#), [Esser et al. \[2024\]](#).

Limitations and broader impact of our study are discussed in Appendix B.

References

- SN Afriat. Theory of maxima and the method of lagrange. *SIAM Journal on Applied Mathematics*, 20(3):343–357, 1971.
- Brandon Amos. On amortizing convex conjugates for optimal transport. In *The Eleventh International Conference on Learning Representations*, 2023. URL https://openreview.net/forum?id=TQ5WUwS_4ai.
- Brandon Amos, Lei Xu, and J Zico Kolter. Input convex neural networks. In *International Conference on Machine Learning*, pages 146–155. PMLR, 2017.
- Arip Asadulaev, Alexander Korotin, Vage Egiazarian, Petr Mokrov, and Evgeny Burnaev. Neural optimal transport with general cost functionals. In *The Twelfth International Conference on Learning Representations*, 2024. URL <https://openreview.net/forum?id=gIiz7tBtYZ>.
- Jean-David Benamou and Yann Brenier. A computational fluid mechanics solution to the monge-kantorovich mass transfer problem. *Numerische Mathematik*, 84(3):375–393, 2000.
- Espen Bernton, Pierre E Jacob, Mathieu Gerber, and Christian P Robert. On parameter estimation with the wasserstein distance. *Information and Inference: A Journal of the IMA*, 8(4):657–676, 2019.
- Charlotte Bunne, Andreas Krause, and Marco Cuturi. Supervised training of conditional monge maps. *Advances in Neural Information Processing Systems*, 35:6859–6872, 2022.
- Hanqun Cao, Cheng Tan, Zhangyang Gao, Yilun Xu, Guangyong Chen, Pheng-Ann Heng, and Stan Z Li. A survey on generative diffusion models. *IEEE Transactions on Knowledge and Data Engineering*, 2024.
- Shreyas Chaudhari, Srinivasa Pranav, and José MF Moura. Gradient networks. *arXiv preprint arXiv:2404.07361*, 2024.
- Yize Chen, Yuanyuan Shi, and Baosen Zhang. Optimal control via neural networks: A convex approach. *arXiv preprint arXiv:1805.11835*, 2018.
- Yongxin Chen, Tryphon T Georgiou, and Michele Pavon. On the relation between optimal transport and schrödinger bridges: A stochastic control viewpoint. *Journal of Optimization Theory and Applications*, 169:671–691, 2016.
- Jaemoo Choi, Jaewoong Choi, and Myungjoo Kang. Generative modeling through the semi-dual formulation of unbalanced optimal transport. In *Thirty-seventh Conference on Neural Information Processing Systems*, 2023. URL <https://openreview.net/forum?id=7WQt1J13ex>.
- Max Daniels, Tyler Maunu, and Paul Hand. Score-based generative neural networks for large-scale optimal transport. *Advances in neural information processing systems*, 34:12955–12965, 2021.
- Valentin De Bortoli, James Thornton, Jeremy Heng, and Arnaud Doucet. Diffusion schrödinger bridge with applications to score-based generative modeling. *Advances in Neural Information Processing Systems*, 34:17695–17709, 2021.
- John R Dormand and Peter J Prince. A family of embedded runge-kutta formulae. *Journal of computational and applied mathematics*, 6(1):19–26, 1980.
- Patrick Esser, Sumith Kulal, Andreas Blattmann, Rahim Entezari, Jonas Müller, Harry Saini, Yam Levi, Dominik Lorenz, Axel Sauer, Frederic Boesel, et al. Scaling rectified flow transformers for high-resolution image synthesis. *arXiv preprint arXiv:2403.03206*, 2024.
- Jiaojiao Fan, Amirhossein Taghvaei, and Yongxin Chen. Scalable computations of wasserstein barycenter via input convex neural networks. *arXiv preprint arXiv:2007.04462*, 2020.
- Jiaojiao Fan, Shu Liu, Shaojun Ma, Hao-Min Zhou, and Yongxin Chen. Neural monge map estimation and its applications. *Transactions on Machine Learning Research*, 2023. ISSN 2835-8856. URL <https://openreview.net/forum?id=2mZSlQscj3>. Featured Certification.

- Aude Genevay, Marco Cuturi, Gabriel Peyré, and Francis Bach. Stochastic optimization for large-scale optimal transport. *Advances in neural information processing systems*, 29, 2016.
- Nikita Gushchin, Sergei Kholkin, Evgeny Burnaev, and Alexander Korotin. Light and optimal schrödinger bridge matching. *arXiv preprint arXiv:2402.03207*, 2024a.
- Nikita Gushchin, Alexander Kolesov, Alexander Korotin, Dmitry P Vetrov, and Evgeny Burnaev. Entropic neural optimal transport via diffusion processes. *Advances in Neural Information Processing Systems*, 36, 2024b.
- J Hiriart-Urruty and Yves Lucet. Parametric computation of the legendre-fenchel conjugate with application to the computation of the moreau envelope. *Journal of Convex Analysis*, 14(3):657, 2007.
- Pieter-Jan Hoedt and Günter Klambauer. Principled weight initialisation for input-convex neural networks. *Advances in Neural Information Processing Systems*, 36, 2024.
- Chin-Wei Huang, Ricky T. Q. Chen, Christos Tsirigotis, and Aaron Courville. Convex potential flows: Universal probability distributions with optimal transport and convex optimization. In *International Conference on Learning Representations*, 2021. URL <https://openreview.net/forum?id=te7PVH1sPxJ>.
- Tero Karras, Samuli Laine, and Timo Aila. A style-based generator architecture for generative adversarial networks. In *Proceedings of the IEEE/CVF conference on computer vision and pattern recognition*, pages 4401–4410, 2019.
- Alexander Korotin, Vage Egiazarian, Arip Asadulaev, Alexander Safin, and Evgeny Burnaev. Wasserstein-2 generative networks. *arXiv preprint arXiv:1909.13082*, 2019.
- Alexander Korotin, Lingxiao Li, Aude Genevay, Justin M Solomon, Alexander Filippov, and Evgeny Burnaev. Do neural optimal transport solvers work? a continuous wasserstein-2 benchmark. *Advances in neural information processing systems*, 34:14593–14605, 2021a.
- Alexander Korotin, Lingxiao Li, Justin Solomon, and Evgeny Burnaev. Continuous wasserstein-2 barycenter estimation without minimax optimization. *arXiv preprint arXiv:2102.01752*, 2021b.
- Alexander Korotin, Vage Egiazarian, Lingxiao Li, and Evgeny Burnaev. Wasserstein iterative networks for barycenter estimation. *Advances in Neural Information Processing Systems*, 35: 15672–15686, 2022.
- Alexander Korotin, Nikita Gushchin, and Evgeny Burnaev. Light schrödinger bridge. In *The Twelfth International Conference on Learning Representations*, 2023a.
- Alexander Korotin, Daniil Selikhanovych, and Evgeny Burnaev. Kernel neural optimal transport. In *The Eleventh International Conference on Learning Representations*, 2023b. URL https://openreview.net/forum?id=Zuc_MHtUma4.
- Alexander Korotin, Daniil Selikhanovych, and Evgeny Burnaev. Neural optimal transport. In *The Eleventh International Conference on Learning Representations*, 2023c. URL <https://openreview.net/forum?id=d8CBRLWNkqH>.
- Maciej Ławryńczuk. Input convex neural networks in nonlinear predictive control: A multi-model approach. *Neurocomputing*, 513:273–293, 2022.
- Christian Léonard. A survey of the schrödinger problem and some of its connections with optimal transport. *arXiv preprint arXiv:1308.0215*, 2013.
- Yaron Lipman, Ricky TQ Chen, Heli Ben-Hamu, Maximilian Nickel, and Matt Le. Flow matching for generative modeling. *arXiv preprint arXiv:2210.02747*, 2022.
- Qiang Liu. Rectified flow: A marginal preserving approach to optimal transport. *arXiv preprint arXiv:2209.14577*, 2022.
- Xingchao Liu, Chengyue Gong, and Qiang Liu. Flow straight and fast: Learning to generate and transfer data with rectified flow. *arXiv preprint arXiv:2209.03003*, 2022.

- Xingchao Liu, Xiwen Zhang, Jianzhu Ma, Jian Peng, and Qiang Liu. InstafLOW: One step is enough for high-quality diffusion-based text-to-image generation. *arXiv preprint arXiv:2309.06380*, 2023.
- Ashok Makkuva, Amirhossein Taghvaei, Sewoong Oh, and Jason Lee. Optimal transport mapping via input convex neural networks. In *International Conference on Machine Learning*, pages 6672–6681. PMLR, 2020.
- Petr Mokrov, Alexander Korotin, Alexander Kolesov, Nikita Gushchin, and Evgeny Burnaev. Energy-guided entropic neural optimal transport. In *The Twelfth International Conference on Learning Representations*, 2024. URL <https://openreview.net/forum?id=d6tUsZeVs7>.
- Stanislav Pidhorskyi, Donald A Adjeroh, and Gianfranco Doretto. Adversarial latent autoencoders. In *Proceedings of the IEEE/CVF Conference on Computer Vision and Pattern Recognition*, pages 14104–14113, 2020.
- Aram-Alexandre Pooladian, Heli Ben-Hamu, Carles Domingo-Enrich, Brandon Amos, Yaron Lipman, and Ricky T. Q. Chen. Multisample flow matching: Straightening flows with minibatch couplings, 2023.
- Jack Richter-Powell, Jonathan Lorraine, and Brandon Amos. Input convex gradient networks. *arXiv preprint arXiv:2111.12187*, 2021.
- Litu Rout, Alexander Korotin, and Evgeny Burnaev. Generative modeling with optimal transport maps. In *International Conference on Learning Representations*, 2022. URL <https://openreview.net/forum?id=5JdLZg346Lw>.
- Vivien Seguy, Bharath Bhushan Damodaran, Rémi Flamary, Nicolas Courty, Antoine Rolet, and Mathieu Blondel. Large-scale optimal transport and mapping estimation. *arXiv preprint arXiv:1711.02283*, 2017.
- Yuyang Shi, Valentin De Bortoli, Andrew Campbell, and Arnaud Doucet. Diffusion schrödinger bridge matching. *Advances in Neural Information Processing Systems*, 36, 2024.
- Jan Stanczuk, Christian Etmann, Lisa Maria Kreusser, and Carola-Bibiane Schönlieb. Wasserstein gans work because they fail (to approximate the wasserstein distance). *arXiv preprint arXiv:2103.01678*, 2021.
- Amirhossein Taghvaei and Amin Jalali. 2-wasserstein approximation via restricted convex potentials with application to improved training for gans. *arXiv preprint arXiv:1902.07197*, 2019.
- Alexander Tong, Nikolay Malkin, Guillaume Hugué, Yanlei Zhang, Jarrid Rector-Brooks, Kilian Fatras, Guy Wolf, and Yoshua Bengio. Conditional flow matching: Simulation-free dynamic optimal transport. *arXiv preprint arXiv:2302.00482*, 2(3), 2023.
- Nazarii Tupitsa, Pavel Dvurechensky, Darina Dvinskikh, and Alexander Gasnikov. Numerical methods for large-scale optimal transport. *arXiv preprint arXiv:2210.11368*, 2022.
- Théo Uscidda and Marco Cuturi. The monge gap: A regularizer to learn all transport maps. In *International Conference on Machine Learning*, pages 34709–34733. PMLR, 2023.
- Bryan Van Scoy, Randy A Freeman, and Kevin M Lynch. The fastest known globally convergent first-order method for minimizing strongly convex functions. *IEEE Control Systems Letters*, 2(1): 49–54, 2017.
- Francisco Vargas, Pierre Thodoroff, Austen Lamacraft, and Neil Lawrence. Solving schrödinger bridges via maximum likelihood. *Entropy*, 23(9):1134, 2021.
- Cédric Villani. *Topics in optimal transportation*, volume 58. American Mathematical Soc., 2021.
- Hanshu Yan, Xingchao Liu, Jiachun Pan, Jun Hao Liew, Qiang Liu, and Jiashi Feng. Perflow: Piecewise rectified flow as universal plug-and-play accelerator, 2024.
- Shu Yang and B Wayne Bequette. Optimization-based control using input convex neural networks. *Computers & Chemical Engineering*, 144:107143, 2021.
- Jun-Yan Zhu, Taesung Park, Phillip Isola, and Alexei A Efros. Unpaired image-to-image translation using cycle-consistent adversarial networks. In *Proceedings of the IEEE international conference on computer vision*, pages 2223–2232, 2017.

A Proofs

Proposition 1 (Simplified OFM Loss). *We can simplify (16) to a more suitable form:*

$$\mathcal{L}_{OFM}^\pi(\Psi) = \int_0^1 \left\{ \int_{\mathbb{R}^D \times \mathbb{R}^D} \left\| \frac{(\phi_t^\Psi)^{-1}(x_t) - x_0}{t} \right\|^2 \pi(x_0, x_1) dx_0 dx_1 \right\} dt, x_t = (1-t)x_0 + tx_1.$$

Proof. By definition $\mathcal{L}_{OFM}^\pi(\Psi)$ equals to

$$\mathcal{L}_{OFM}^\pi(\Psi) := \int_0^1 \left\{ \int_{\mathbb{R}^D \times \mathbb{R}^D} \|u_t^\Psi(x_t) - (x_1 - x_0)\|^2 \pi(x_0, x_1) dx_0 dx_1 \right\} dt, x_t = (1-t)x_0 + tx_1.$$

For fixed points x_0, x_1 and time t in integrand, we find a point $z_0 = (\phi_t^\Psi)^{-1}(x_t)$ such that in moment $t \in [0, 1]$ it is transported to point $x_t = (1-t)x_0 + tx_1$. This point z_0 satisfies equality

$$x_t = t\nabla\Psi(z_0) + (1-t)z_0.$$

We define the vector field u_t^Ψ as

$$u_t^\Psi(x_t) = \nabla\Psi(z_0) - z_0 = \frac{x_t - z_0}{t}.$$

Putting $u_t^\Psi(x_t)$ in the integrand of (21), we obtain simplified integrand

$$\begin{aligned} \|x_1 - x_0 - u_t^\Psi(x_t)\|^2 &= \left\| x_1 - x_0 - \left(\frac{x_t - z_0}{t} \right) \right\|^2 \\ &= \frac{1}{t^2} \|tx_1 - tx_0 - ((1-t)x_0 + tx_1) + z_0\|^2 \\ &= \frac{1}{t^2} \|z_0 - x_0\|^2 = \left\| \frac{(\phi_t^\Psi)^{-1}(x_t) - x_0}{t} \right\|^2. \end{aligned}$$

□

Lemma 1 (Main Integration Lemma). *For any two points $x_0, x_1 \in \mathbb{R}^D$ and a convex function Ψ , the following equality holds true:*

$$\int_0^1 \|u_t^\Psi(x_t) - (x_1 - x_0)\|^2 dt = 2 \cdot [\Psi(x_0) + \bar{\Psi}(x_1) - \langle x_0, x_1 \rangle]. \quad (21)$$

Proof. In order to find a point $z_0(t) = z_0 = (\phi_t^\Psi)^{-1}(x_t)$ for fixed x_0, x_1 such that in moment $t \in (0, 1)$ it is transported to point $x_t = (1-t)x_0 + tx_1$ we need to satisfy equality

$$x_t = t\nabla\Psi(z_0) + (1-t)z_0. \quad (22)$$

We use the simplified loss form from Proposition 1, i.e.,

$$\|u_t^\Psi(x_t) - (x_1 - x_0)\|^2 = \frac{1}{t^2} \|z_0 - x_0\|^2.$$

Next, we integrate (21) w.r.t. time t from 0 excluding to 1 excluding (This exclusion does not change the integral). We notice, that set of points $z_0(t) = (\phi_t^\Psi)^{-1}(x_t), t \in (0, 1)$ forms a curve in \mathbb{R}^D with parameter t , and one can integrate along it. The limits of integration along the curve $z_0(t)$ are

$$z_0(t)|_{t=0} = x_0, \quad z_0(t)|_{t=1} = \nabla\bar{\Psi}(x_1). \quad (23)$$

Further, we change the time variable t to $s = \frac{1}{t}, ds = -\frac{dt}{t^2}$ and get

$$\int_0^1 \frac{1}{t^2} \|z_0(t) - x_0\|^2 dt = - \int_{+\infty}^1 \|z_0(s) - x_0\|^2 ds = - \int_{+\infty}^1 \langle z_0(s) - x_0, z_0(s) - x_0 \rangle ds. \quad (24)$$

In the condition (22), we also consider the change

$$\begin{aligned}
x_t = t\nabla\Psi(z_0) + (1-t)z_0 &= (1-t)x_0 + tx_1, \\
t(\nabla\Psi(z_0) - x_1) &= (1-t)(x_0 - z_0), \\
(\nabla\Psi(z_0) - x_1) &= \left(\frac{1}{t} - 1\right)(x_0 - z_0), \\
(\nabla\Psi(z_0) - x_1) &= (s-1)(x_0 - z_0).
\end{aligned}$$

We make one more substitution from s to $s' = \frac{1}{s-1}$, $ds' = -\frac{ds}{(s-1)^2} = -(s')^2 ds$ and obtain

$$\begin{aligned}
(\nabla\Psi(z_0) - x_1) &= (s-1)(x_0 - z_0), \\
(\nabla\Psi(z_0) - x_1) &= \frac{(x_0 - z_0)}{s'}, \\
s'(\nabla\Psi(z_0) - x_1) &= (x_0 - z_0).
\end{aligned} \tag{25}$$

The integral (24) changes as

$$\begin{aligned}
-\int_{+\infty}^1 \|x_0 - z_0(s)\|^2 ds &= \int_0^{\infty} \left\langle \frac{x_0 - z_0(s')}{s'}, \frac{x_0 - z_0(s')}{s'} \right\rangle ds' \\
&= \int_0^{\infty} \langle \nabla\Psi(z_0(s')) - x_1, \nabla\Psi(z_0(s')) - x_1 \rangle ds'.
\end{aligned}$$

In order to eliminate differential ds' , we take differential from both sides of (25) w.r.t. s'

$$\begin{aligned}
d[(\nabla\Psi(z_0) - x_1)s'] &= d[x_0 - z_0], \\
s'\nabla^2\Psi(z_0)dz_0 + (\nabla\Psi(z_0) - x_1)ds' &= -dz_0, \\
(\nabla\Psi(z_0) - x_1)ds' &= -(s'\nabla^2\Psi(z_0) + I)dz_0.
\end{aligned}$$

Next, we continue

$$\begin{aligned}
\|x_1 - x_0 - u_t^\Psi(x_t)\|^2 &= \int_0^{\infty} \langle \nabla\Psi(z_0) - x_1, \nabla\Psi(z_0) - x_1 \rangle ds' \\
&= \int_{z_0}^{\infty} \langle x_1 - \nabla\Psi(z_0), (s'\nabla^2\Psi(z_0) + I)dz_0 \rangle \\
&= \int_{z_0}^{\infty} \langle x_1 - \nabla\Psi(z_0), dz_0 \rangle + \int_{z_0}^{\infty} \langle s'(x_1 - \nabla\Psi(z_0)), \nabla^2\Psi(z_0)dz_0 \rangle \\
&\stackrel{(25)}{=} \int_{z_0}^{\infty} \langle x_1 - \nabla\Psi(z_0), dz_0 \rangle + \int_{z_0}^{\infty} \langle z_0 - x_0, \nabla^2\Psi(z_0)dz_0 \rangle.
\end{aligned} \tag{26}$$

We notice that

$$\begin{aligned}
d\langle z_0, \nabla\Psi(z_0) \rangle &= \langle z_0, \nabla^2\Psi(z_0)dz_0 \rangle + \langle dz_0, \nabla\Psi(z_0) \rangle, \\
\langle z_0, \nabla^2\Psi(z_0)dz_0 \rangle &= d\langle z_0, \nabla\Psi(z_0) \rangle - \langle \nabla\Psi(z_0), dz_0 \rangle.
\end{aligned}$$

As a consequence, we write down

$$\begin{aligned}
(26) &= \int_{z_0} \langle x_1 - \nabla \Psi(z_0), dz_0 \rangle + \int_{z_0} \langle z_0 - x_0, \nabla^2 \Psi(z_0) dz_0 \rangle \\
&= \int_{z_0} \langle x_1, dz_0 \rangle - \int_{z_0} \langle \nabla \Psi(z_0), dz_0 \rangle \\
&+ \int_{z_0} d\langle z_0, \nabla \Psi(z_0) \rangle - \int_{z_0} \langle \nabla \Psi(z_0), dz_0 \rangle - \int_{z_0} \langle x_0, \nabla^2 \Psi(z_0) dz_0 \rangle \\
&= \int_{z_0} \langle x_1, dz_0 \rangle - 2 \int_{z_0} \langle \nabla \Psi(z_0), dz_0 \rangle + \int_{z_0} d\langle z_0, \nabla \Psi(z_0) \rangle - \int_{z_0} \langle x_0, \nabla^2 \Psi(z_0) dz_0 \rangle. \quad (27)
\end{aligned}$$

Under all integrals we have closed form differentials

$$\begin{aligned}
\langle x_1, dz_0 \rangle &= d\langle x_1, z_0 \rangle, \\
\langle \nabla \Psi(z_0), dz_0 \rangle &= d\Psi(z_0), \\
\langle x_0, \nabla^2 \Psi(z_0) dz_0 \rangle &= d\langle x_0, \nabla \Psi(z_0) \rangle.
\end{aligned}$$

We integrate them from initial point x_0 to the final $\nabla \bar{\Psi}(x_1)$ according to limits (23) and get

$$\begin{aligned}
(27) &= \int_{z_0} d\langle x_1, z_0 \rangle - 2 \int_{z_0} d\Psi(z_0) + \int_{z_0} d\langle z_0, \nabla \Psi(z_0) \rangle - \int_{z_0} d\langle x_0, \nabla \Psi(z_0) \rangle \\
&= \langle x_1, \nabla \bar{\Psi}(x_1) \rangle - \langle x_1, x_0 \rangle + 2(\Psi(x_0) - \Psi(\nabla \bar{\Psi}(x_1))) + \langle (\nabla \bar{\Psi}(x_1), \nabla \Psi(\nabla \bar{\Psi}(x_1))) \rangle \\
&- \langle x_0, \nabla \Psi(x_0) \rangle + \langle x_0, \nabla \Psi(x_0) \rangle - \langle x_0, \nabla \Psi(\nabla \bar{\Psi}(x_1)) \rangle. \quad (28)
\end{aligned}$$

Finally, we use properties of conjugate functions:

- Invertability:

$$\nabla \Psi(\nabla \bar{\Psi}(x_1)) = \nabla \Psi(\nabla \Psi^{-1}(x_1)) = x_1, \quad \forall x_1 \in \mathbb{R}^D,$$

- Fenchel-Young's equality:

$$\Psi(\nabla \bar{\Psi}(x_1)) + \bar{\Psi}(x_1) = \langle \nabla \bar{\Psi}(x_1), x_1 \rangle, \quad \forall x_1 \in \mathbb{R}^D.$$

We simplify (28) to

$$\begin{aligned}
(28) &= \langle x_1, \nabla \bar{\Psi}(x_1) \rangle - \langle x_1, x_0 \rangle + 2(\Psi(x_0) + \bar{\Psi}(x_1) - \langle \nabla \bar{\Psi}(x_1), x_1 \rangle) + \langle (\nabla \bar{\Psi}(x_1), x_1) \rangle \\
&- \langle x_0, \nabla \Psi(x_0) \rangle + \langle x_0, \nabla \Psi(x_0) \rangle - \langle x_0, x_1 \rangle \\
&= 2[\Psi(x_0) + \bar{\Psi}(x_1) - \langle x_0, x_1 \rangle].
\end{aligned}$$

□

Theorem 1 (OFM and OT connection). *Let us consider two distributions $p_0, p_1 \in \mathcal{P}_{ac,2}(\mathbb{R}^D)$ and any transport plan $\pi \in \Pi(p_0, p_1)$ between them. Then, losses $\mathcal{L}_{OT}(\Psi)$ and $\mathcal{L}_{OFM}^\pi(\Psi)$, defined in (4) and (16), respectively, have the same minimizers, i.e.,*

$$\arg \min_{\text{convex } \Psi} \mathcal{L}_{OFM}^\pi(\Psi) = \arg \min_{\text{convex } \Psi} \mathcal{L}_{OT}(\Psi).$$

Proof. Main Integration Lemma 1 states that for any fixed points x_0, x_1 we have

$$\int_0^1 \|x_1 - x_0 - u_{t,\Psi}(x_t)\|^2 dt = 2[\Psi(x_0) + \bar{\Psi}(x_1) - \langle x_0, x_1 \rangle].$$

Taking math expectation over any plan π (integration w.r.t. points $x_0, x_1 \sim \pi$) gives

$$\underbrace{\mathbb{E}_{x_0, x_1 \sim \pi} \int_0^1 \|u_t^\Psi(x_t) - (x_1 - x_0)\|^2 dt}_{=\mathcal{L}_{OFM}^\pi(\Psi)} = 2 \cdot \underbrace{\mathbb{E}_{x_0, x_1 \sim \pi} [\Psi(x_0) + \bar{\Psi}(x_1)]}_{=\mathcal{L}_{OT}(\Psi)} - 2 \cdot \underbrace{\mathbb{E}_{x_0, x_1 \sim \pi} [\langle x_0, x_1 \rangle]}_{=:\text{CONST}'(\pi)},$$

where $\text{CONST}'(\pi)$ does not depend on Ψ . Hence, both minimums of OFM loss $\mathcal{L}_{OFM}^\pi(\Psi)$ and of OT dual form loss $\mathcal{L}_{OT}(\Psi)$ are achieved at the same functions. \square

Proposition 2 (Intractable Distance). *The distance (19) between an arbitrary vector field u and OT field u^* equals to the FM loss from (10) with the optimal plan π^* , i.e.,*

$$\text{DIST}(u, u^*) = \mathcal{L}_{FM}^{\pi^*}(u) - \underbrace{\mathcal{L}_{FM}^{\pi^*}(u^*)}_{=0}.$$

Proof. We recall the definitions of $\text{DIST}(u, u^*)$ (19) and FM loss $\mathcal{L}_{FM}^{\pi^*}(u)$ (10):

$$\begin{aligned} \text{DIST}(u, u^*) &:= \int_0^1 \int_{\mathbb{R}^D} \|u_t(x_t) - u_t^*(x_t)\|^2 \underbrace{\phi_t^* \# p_0(x_t)}_{:=p_t^*(x_t)} dx_t dt, \\ \mathcal{L}_{FM}^{\pi^*}(u) &:= \int_0^1 \left\{ \int_{\mathbb{R}^D \times \mathbb{R}^D} \|u_t(x_t) - (x_1 - x_0)\|^2 \pi^*(x_0, x_1) dx_0 dx_1 \right\}, x_t = (1-t)x_0 + tx_1. \end{aligned}$$

In the optimal plan π^* , each point x_0 almost surely goes to the single point $\nabla \Psi^*(x_0)$. Hence, in FM loss, we can leave only integration over initial points x_0 substituting $x_1 = \nabla \Psi^*(x_0)$, i.e, for fixed time t

$$\begin{aligned} \int_{\mathbb{R}^D \times \mathbb{R}^D} \|u_t(x_t) - (x_1 - x_0)\|^2 \pi^*(x_0, x_1) dx_0 dx_1 &= \int_{\mathbb{R}^D} \|u_t(x_t) - (\nabla \Psi^*(x_0) - x_0)\|^2 p_0(x_0) dx_0. \\ x_t &= (1-t)x_0 + t\nabla \Psi^*(x_0). \end{aligned} \quad (29)$$

We notice that dynamic OT vector field $u^* = u^{\Psi^*}$ is the optimal one with potential Ψ^* . Moreover, for any point $x_t = (1-t)x_0 + t\nabla \Psi^*(x_0)$ generated by u^* , we can calculate $u_t^*(x_t) = u_t^{\Psi^*}(x_t) = \nabla \Psi^*(x_0) - x_0$. It is the same expression as from (29), i.e.,

$$\begin{aligned} (29) &= \int_{\mathbb{R}^D} \|u_t(x_t) - (\nabla \Psi^*(x_0) - x_0)\|^2 p_0(x_0) dx_0 \\ &= \int_{\mathbb{R}^D} \|u_t(x_t) - u_t^*(x_t)\|^2 p_0(x_0) dx_0. \end{aligned} \quad (30)$$

Finally, we change the variable x_0 to $x_t = \phi_t^*(x_0)$, and probability changes as $p_0(x_0) dx_0 = \phi_t^* \# p_0(x_t) dx_t = p_t^*(x_t) dx_t$. In new variables, we obtain the result

$$\int_{\mathbb{R}^D \times \mathbb{R}^D} \|u_t(x_t) - (x_1 - x_0)\|^2 \pi^*(x_0, x_1) dx_0 dx_1 = \int_{\mathbb{R}^D} \|u_t(x_t) - u_t^*(x_t)\|^2 p_t^*(x_t) dx_t.$$

Hence, the integration over time t gives the desired equality

$$\text{DIST}(u, u^*) = \mathcal{L}_{FM}^{\pi^*}(u)$$

and $\mathcal{L}_{FM}^{\pi^*}(u^*) = \text{DIST}(u^*, u^*) = 0$. \square

Proposition 3 (Tractable Distance For OFM). *The distance $\text{DIST}(u^\Psi, u^{\Psi^*})$ between an **optimal** vector field u^Ψ generated by a convex function Ψ and the vector field u^{Ψ^*} with the Brenier potential Ψ^* can be evaluated directly via OFM loss from (16) and **any** plan π :*

$$\text{DIST}(u^\Psi, u^{\Psi^*}) = \mathcal{L}_{OFM}^\pi(\Psi) - \mathcal{L}_{OFM}^\pi(\Psi^*). \quad (31)$$

Proof. For the vector field u^Ψ , we apply the formula for intractable distance from Proposition 3, i.e.,

$$\text{DIST}(u^\Psi, u^{\Psi^*}) = \mathcal{L}_{OFM}^{\pi^*}(\Psi) - \mathcal{L}_{OFM}^{\pi^*}(\Psi^*).$$

According to Main Integration Lemma 1, for any plan π and convex function Ψ , we have equality

$$\underbrace{\mathbb{E}_{x_0, x_1 \sim \pi} \int_0^1 \|u_t^\Psi(x_t) - (x_1 - x_0)\|^2 dt}_{=\mathcal{L}_{OFM}^\pi(\Psi)} = 2 \cdot \underbrace{\mathbb{E}_{x_0, x_1 \sim \pi} [\Psi(x_0) + \bar{\Psi}(x_1)]}_{=\mathcal{L}_{OT}(\Psi)} - \underbrace{2 \cdot \mathbb{E}_{x_0, x_1 \sim \pi} [\langle x_0, x_1 \rangle]}_{=:\text{CONST}'(\pi)}.$$

Since $\text{CONST}'(\pi)$ does not depend on Ψ , we have the same constant with $\Psi = \Psi^*$ and can eliminate it, i.e.,

$$\begin{aligned} \mathcal{L}_{OFM}^\pi(\Psi) &= 2 \cdot \mathcal{L}_{OT}(\Psi) - \text{CONST}'(\pi) \\ \mathcal{L}_{OFM}^\pi(\Psi^*) &= 2 \cdot \mathcal{L}_{OT}(\Psi^*) - \text{CONST}'(\pi) \\ &\Downarrow \\ \mathcal{L}_{OFM}^\pi(\Psi) - \mathcal{L}_{OFM}^\pi(\Psi^*) &= 2 \cdot \mathcal{L}_{OT}(\Psi) - 2 \cdot \mathcal{L}_{OT}(\Psi^*). \end{aligned}$$

The right part of (32) does not depend on a plan π , thus, the left part is invariant for any plan including optimal plan π^* , i.e.,

$$\mathcal{L}_{OFM}^\pi(\Psi) - \mathcal{L}_{OFM}^\pi(\Psi^*) = \mathcal{L}_{OFM}^{\pi^*}(\Psi) - \mathcal{L}_{OFM}^{\pi^*}(\Psi^*) = \text{DIST}(u^\Psi, u^{\Psi^*}).$$

□

Proposition 4 (Explicit Loss Gradient Formula). *The gradient of \mathcal{L}_{OFM}^π can be calculated as*

$$\begin{aligned} z_0 &= \text{NO-GRAD} \left\{ (\phi_t^{\Psi_\theta})^{-1}(x_t) \right\}, \\ \frac{d\mathcal{L}_{OFM}^\pi}{d\theta} &:= \frac{d}{d\theta} \mathbb{E}_{t; x_0, x_1 \sim \pi} \left\langle \text{NO-GRAD} \left\{ 2 \left(t\nabla^2 \Psi_\theta(z_0) + (1-t)I \right)^{-1} \frac{(x_0 - z_0)}{t} \right\}, \nabla \Psi_\theta(z_0) \right\rangle, \end{aligned}$$

where variables under NO-GRAD remain constants during differentiation.

Proof. Point $z_0 = (\phi_t^{\Psi_\theta})^{-1}(x_t)$ now depends on parameters θ . We differentiate the integrand from the simplified OFM loss (17) for fixed points x_0, x_1 and time t , i.e.,

$$d \left(\frac{1}{t^2} \|z_0 - x_0\|^2 \right) = 2 \left\langle \frac{z_0 - x_0}{t^2}, \frac{dz_0}{d\theta} d\theta \right\rangle. \quad (32)$$

For point z_0 , the equation (22) holds true:

$$x_t = (1-t)z_0 + t\nabla \Psi_\theta(z_0). \quad (33)$$

We differentiate (33) w.r.t. θ and obtain

$$\begin{aligned} 0 &= (1-t) \frac{dz_0}{d\theta} + t\nabla^2 \Psi_\theta(z_0) \frac{dz_0}{d\theta} + t \frac{\partial \nabla \Psi_\theta}{\partial \theta}(z_0), \\ \frac{dz_0}{d\theta} &= - \left(t\nabla^2 \Psi_\theta(z_0) + (1-t)I \right)^{-1} \cdot t \frac{\partial \nabla \Psi_\theta}{\partial \theta}(z_0). \end{aligned}$$

Therefore, we have

$$\begin{aligned} (32) &= \left\langle 2 \frac{x_0 - z_0}{t}, \left(t\nabla^2 \Psi_\theta(z_0) + (1-t)I \right)^{-1} \frac{\partial \nabla \Psi_\theta}{\partial \theta}(z_0) d\theta \right\rangle \\ &= \left\langle 2 \left(t\nabla^2 \Psi_\theta(z_0) + (1-t)I \right)^{-1} \frac{(x_0 - z_0)}{t}, \frac{\partial \nabla \Psi_\theta}{\partial \theta}(z_0) d\theta \right\rangle. \end{aligned} \quad (34)$$

Now the differentiation over θ is located only in the right part of (34) in the term $\frac{\partial \nabla \Psi_\theta}{\partial \theta}$. Hence, point z_0 and the left part of (34) can be considered as constants during differentiation. To get the gradient of OFM loss we also need to take math expectation over plan π and time t . □

B Limitations and Broader Impact

Flow map inversion. During training, we need to compute $(\phi_t^{\Psi_\theta})^{-1}(\cdot)$ via solving strongly convex subproblem (20). In practice, we approach it by the standard gradient descent (with Adam optimizer), but actually there exist many improved methods to solve such conjugation problems more effectively in both the optimization Van Scoy et al. [2017], Hiriart-Urruty and Lucet [2007] and OT Amos [2023], Makkuva et al. [2020]. This provides a dozen of opportunities for improvement, but leave such advanced methods for future research.

ICNNs. It is known that ICNNs may underperform compared to regular neural networks Korotin et al. [2021a, 2022]. Thus, ICNN parametrization may limit the performance of our OFM. Fortunately, deep learning community actively study ways to improve ICNNs Chaudhari et al. [2024], Bunne et al. [2022], Richter-Powell et al. [2021], Hoedt and Klambauer [2024] due to their growing popularity in various tasks Yang and Bequette [2021], Ławryńczuk [2022], Chen et al. [2018]. We believe that the really expressive ICNN architectures are yet to come.

Hessian inversion. We get the gradient of our OFM loss via formula from Proposition 4. There we have to invert the hessian $\nabla^2\Psi(\cdot)$, which is expensive. We point to addressing this limitation as a promising avenue for future studies.

Broader impact. This paper presents work whose goal is to advance the field of Machine Learning. There are many potential societal consequences of our work, none of which we feel must be specifically highlighted here.

C Experiments details

To implement our proposed approach in practice, we adopt fully-connected ICNN architectures proposed in [Korotin et al., 2019, Appendix B2] (W2GN_ICNN) and [Huang et al., 2021, Appendix E1] (CPF_ICNN). To ensure the convexity, both architectures place some restrictions on the NN’s weights and utilized activation functions, see the particular details in the corresponding papers. We take the advantage of their official repositories:

<https://github.com/iamalexkorotin/Wasserstein2Benchmark;>
[https://github.com/CW-Huang/CP-Flow.](https://github.com/CW-Huang/CP-Flow)

We aggregate the hyper-parameters of our Algorithm 1 and utilized ICNNs for different experiments in Table 2. In all our experiments as the *subOpt* optimizer we use LBFGS (`torch.optim.LBFGS`) with K_{sub} optimization steps and early stopping criteria based on gradient norm. To find the initial point z_0^i (Step 5 of our Algorithm 1), we initialize *subOpt* with $x_{t_i}^i$. As the *Opt* optimizer we adopt Adam with learning rate lr and other hyperparameters set to be default.

Experiment	ICNN architecture Ψ_θ	K	B	lr	K_{sub}
Illustrative 2D	CPF_ICNN, $\mathbb{R}^2 \rightarrow \mathbb{R}$, Softplus, [1024, 1024]	30K	1024	10^{-2}	5
W2 bench., dim. D	W2GN_ICNN, $\mathbb{R}^D \rightarrow \mathbb{R}$, CELU, [128, 128, 64]	30K	1024	10^{-3}	50
ALAE	W2GN_ICNN, $\mathbb{R}^{512} \rightarrow \mathbb{R}$, CELU, [1024, 1024]	10K	128	10^{-3}	10

Table 2: Hyper-parameters of our OFM solvers in different experiments

Minibatch. Similarly to OT-CFM, in some of our experiments we use non-independent initial plans π to improve convergence. We construct π as follows: for independently sampled minibatches X_0, X_1 of the same size B , we build the optimal discrete map and apply it to reorder the pairs of samples. We stress that considering minibatch OT for our method is done exclusively to speed up the training process. Theoretically, our method is agnostic to initial plan π and is guaranteed to have an optimum in dynamic OT solution.

Computation time. In what follows, we provide approximate running times for training our OFM method in different experiments with hyper-parameters provided in Table 2. For Illustrative 2D (*Gaussian*→*Eight Gaussian*) experiment the training takes ≈ 1.5 hours on a single 1080 ti gpu. For Wasserstein-2 benchmark, the computation time depends on the dimensionality $D = 2, 4, \dots, 256$.

Totally, all the benchmark experiments (both with independent and MB plan π) take ≈ 3 days on three A100 gpus. For ALAE experiment, the training stage lasts for ≈ 5 hours on a single 1080 ti.

C.1 Benchmark details

Metrics. Following the authors of the benchmark Korotin et al. [2021a], to assess the quality of retrieved transport map T between p_0 and p_1 , we use *unexplained variance percentage* (UVP): $\mathcal{L}^2\text{-UVP}(T) := 100 \cdot \|T - T^*\|_{\mathcal{L}^2(p_0)}^2 / \text{Var}(p_1)\%$. For values $\mathcal{L}^2\text{-UVP}(T) \approx 0\%$, T approximates T^* , while for values $\geq 100\%$ T is far from optimal. We also calculate the *cosine similarity* between ground truth directions $T^* - \text{id}$ and obtained directions $T - \text{id}$, i.e.,

$$\cos(T - \text{id}, T^* - \text{id}) = \frac{\langle T - \text{id}, T^* - \text{id} \rangle_{\mathcal{L}^2(p_0)}}{\|T - \text{id}\|_{\mathcal{L}^2(p_0)} \cdot \|T^* - \text{id}\|_{\mathcal{L}^2(p_0)}} \in [-1, 1].$$

For good approximations the cosine metric is approaching 1. We estimate $\mathcal{L}^2\text{-UVP}$ and cos metrics with 2^{14} samples from p_0 . Solvers’ results for cos metric are presented in Table 3.

Solver	Solver type	$D=2$	$D=4$	$D=8$	$D=16$	$D=32$	$D=64$	$D=128$	$D=256$
MMv1* Stanczuk et al. [2021]	Dual OT solver	0.99	0.99	0.99	0.99	0.98	0.99	0.99	0.99
	Linear*	0.75	0.80	0.73	0.73	0.76	0.75	0.77	0.77
OT-CFM MB Tong et al. [2023]	Flow Matching	0.999	0.985	0.978	0.968	0.975	0.96	0.949	0.915
RF Liu et al. [2022]		0.87	0.75	0.65	0.67	0.72	0.70	0.70	0.70
c-RF Liu [2022]		0.989	0.83	0.83	0.78	0.778	0.762	0.748	0.73
OFM Ind (Ours)		0.997	0.981	0.98	0.98	0.988	0.95	0.965	0.94
OFM MB (Ours)		0.999	0.984	0.985	0.985	0.992	0.956	0.976	0.96

Table 3: cos values of solvers fitted on high-dimensional benchmarks in dimensions $D = 2, 4, 8, 16, 32, 64, 128, 256$. The best metric over *Flow Matching* solvers is **bolded**. * Metrics for MMv1 and linear baseline are taken from Korotin et al. [2019].

Details of Baseline Solvers Neural networks’ architectures of competing Flow Matching methods and their parameters used in benchmark experiments are presented in Table 4. In this Table, “FC” stands for “fully-connected”.

Solver	Architecture	Activation	Hidden layers	Optimizer	Batch size	Learning rate	Iter. per round * rounds
OT CFM Tong et al. [2023]	FC NN $\mathbb{R}^D \times [0, 1] \rightarrow \mathbb{R}^D$	ReLU	[128, 128, 64]	RMSProp	1024	10^{-3}	200.000
RF Liu et al. [2022]	FC NN $\mathbb{R}^D \times [0, 1] \rightarrow \mathbb{R}^D$	ReLU	[128, 128, 64]	RMSProp	1024	10^{-4}	65.000 * 3
c-RF Liu [2022]	FC NN $\mathbb{R}^D \times [0, 1] \rightarrow \mathbb{R}$	ReLU	[128, 128, 64]	RMSProp	1024	10^{-5}	100.000 * 2

Table 4: Parameters of models fitted on benchmark in dimensions $D = 2, 4, 8, 16, 32, 64, 128, 256$

Time variable t in (c -)RF and OT-CFM’s architectures is added as one more dimensionality in input without special preprocessing. In RF and c -RF, ODE are solved via Explicit Runge-Kutta method of order 5(4) Dormand and Prince [1980] with absolute tolerance $10^{-4} - 10^{-6}$. In OFM and c -RF, gradients over input are calculated via autograd of PyTorch. All algorithms converge in several hours on the single GPU.

Following the authors of RF Liu et al. [2022], we run only 2 – 3 rounds in RF. In further rounds, straightness and metrics change insignificantly, while the error of target distribution learning still accumulates.

Our implementations of OT-CFM Tong et al. [2023] and RF Liu et al. [2022] are based on the official repositories:

<https://github.com/atong01/conditional-flow-matching>
<https://github.com/gnabitab/RectifiedFlow>

Implementation of c -RF follows the RF framework with the modification of optimized NN’s architecture. Instead of $\mathbb{R}^D \times [0, 1] \rightarrow \mathbb{R}^D$ net, we parametrize time-dependent scalar valued model $\mathbb{R}^D \times [0, 1] \rightarrow \mathbb{R}$ which gradients are set to be the vector field.

C.2 Unpaired Image-to-image transfer details

To conduct the experiments with high-dimensional I2I translation empowered with pretrained ALAE autoencoder, we adopt the publicly available code:

<https://github.com/SKholkin/LightSB-Matching>.

Additional qualitative results for our method are provided on Figure 4



Figure 4: Unpaired I2I $Adult \rightarrow Child$ by **our** OFM solver, ALAE 1024×1024 FFHQ latent space. The samples are uncurated.